ADVANCED FUNCTIONAL MATERIALS
www.afm-journal.de

Materials Views
www.MaterialsViews.com

FULL PAPER

Load-Controlled Roll Transfer of Oxide Transistors for Stretchable Electronics

Bhupendra K. Sharma, Bongkyun Jang, Jeong Eun Lee, Sang-Hoon Bae, Tae Woong Kim, Hak-Joo Lee, Jae-Hyun Kim, and Jong-Hyun Ahn**

A stretchable and transparent In-Ga-Zn-O (IGZO) thin film transistors with high electrical performance and scalability is demonstrated. A load-controlled roll transfer method is realized for fully automated and scalable transfer of the IGZO TFTs from a rigid substrate to a nonconventional elastomeric substrate. The IGZO TFTs exhibit high electrical performance under stretching and cyclic tests, demonstrating the potentiality of the load-controlled roll transfer in stretchable electronics. The mechanics of the load-controlled roll transfer is investigated and simulated, and it is shown that the strain level experienced by the active layers of the device can be controlled to well below their maximum fracture level during transfer.

1. Introduction

The integration of transparent electronic devices on non-conventional substrate enables the development of a wide range of applications, including next-generation displays,[1–4] fully conformable biomedical devices,[5–7] smart windows,[8,9] and wearable electronics.[10–14] The most widespread materials used as active components for transparent electronics are oxide semiconductors.[15–20] Currently, indium-gallium-zinc-oxide (IGZO), has drawn a considerable attention as one of the most promising transparent semiconductor candidates for thin film transistor circuitry, due to its higher current driving capability than hydrogenated amorphous silicon (a-Si:H), superior scalability, and high optical transparency.[21–23] The integration of oxide-based thin film transistors (TFTs) on flexible substrate may bring about the practical realization of large-area flexible electronics. Recently, most attempts have been carried out towards the fabrication of IGZO TFTs on flexible substrates by employing low-temperature processing.[24–26] However, the main drawback of this approach is that room-temperature or low-temperature processing can easily affect the quality of the gate dielectric, IGZO channel, electrode contact, and interface between the channel and gate dielectric. Therefore, for better performance, devices have required an annealing process. In addition, the electronic circuitry formed on flexible substrates has been able to bend easily, but cannot twist or stretch. As such, for further development and practical realization of IGZO-based wearable and conformal electronics, the fabrication of IGZO TFTs on stretchable substrate has been demanding and challenging. Stretchable or elastic electronics are entirely different from their conventional counterparts, especially for conventional inorganic material with poor mechanical robustness, as unique shape, design and stretching ability are required for interconnections among the active device islands.[27,28]

An alternative approach for overcoming the drawbacks of direct fabrication of IGZO TFTs on nonconventional substrates involves first fabricating the TFTs on conventional, high-temperature-resistant rigid substrates, such as Si wafer and glass, followed by transfer onto nonconventional, stretchable substrates. So far, no attempt has been made towards the embedding of IGZO TFTs after the high-temperature fabrication process required for good electrical performance, on nonconventional substrates in order to integrate stretching ability.

Recently, the roll-to-roll approach has attracted considerable attention for large-scale production with high-throughput, low cost, and time effectiveness. We previously demonstrated the roll-to-roll process for large-area (30-inch) graphene.[29] Lee et al. also used this approach for surface nanotexturing.[30] Tavares et al. and Yang et al. demonstrated the transfer of one-dimensional nanofibers and silicon arrays with manual rollers,[31,32] but none have applied this process to transferring electronic circuitry from rigid to nonconventional substrates for the fabrication of stretchable electronics. In an earlier report,[33] we demonstrated a manual plate-to-plate transfer method, which was not very controlled and compatible for large-area stretchable electronics. In the present work, a load-controlled roll transfer method is introduced in a very controlled manner for practical realization of large-area, flexible, and stretchable electronics, which seems

Dr. B. K. Sharma, J. E. Lee, S.-H. Bae, Prof. J.-H. Ahn
School of Advanced Materials Science and Engineering
SKKU Advanced Institute of Nanotechnology
Sungkyunkwan University
Suwon, 440-476, Korea
E-mail: ahnj@skku.edu

B. Jang, Dr. H.-J. Lee, Dr. J.-H. Kim
Department of Nano Mechanics
Nano-Convergence Mechanical Systems Research Division
Korea Institute of Machinery & Materials
156, Gajeongbuk-ro, Yuseong-gu, Daejeon, 305-343, Korea
E-mail: jaehkim@kimm.re.kr
Dr. T. W. Kim
Next Generation B/P Development Team
OLED R&D Center
Samsung Mobile Display, Suwon, 440-476, Korea

DOI: 10.1002/adfm.201202519

© 2013 WILEY-VCH Verlag GmbH & Co. KGaA, Weinheim

to be more feasible. The primary advantage of a roll-based process is its well-defined contact area. The roll-stamp has a one-dimensional contact region with very small width, but the planar stamp has a two-dimensional one. By translating the one-dimensional contact region on a substrate, the whole area of the substrate can be accessed, thus, scaling up the process is straightforward. The one-dimensional contact region is more easily controllable than a two-dimensional one using a feedback control of the contact load. For the scalable roll transfer of thin film electronics, it is necessary to control the contact load between the roller and thin film devices with high resolution, since the thin film devices are fragile and are easily fractured, due to fluctuation of the contact load induced by imperfection or misalignment of the roller, dust particles, and thickness variation of the stamp and devices. This cannot be realized using a manual stamp, and there is no literature on the mechanics of roll transfer or a roller controlling method for the realization of transfer for thin film electronics.

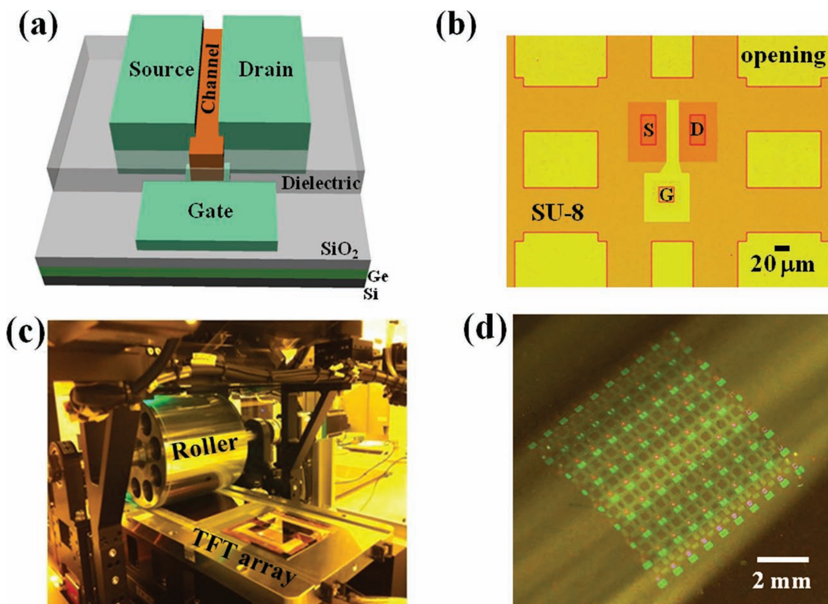

Figure 1. Schematic and optical representation of IGZO based TFTs at different steps during the transfer by roller. a) Schematic cross-section of IGZO TFT device. b) Optical image of top view of SU-8-encapsulated IGZO TFT. c) Photograph during transfer of device by automated roller. d) Photograph of TFT arrays attached to the roller surface.

In the present study, we demonstrate the fabrication method of stretchable and transparent IGZO TFT arrays on a stretchable substrate. We developed a roll transfer system capable of real-time feedback control of the contact load, and showed that the load-controlled roll transfer was very critical for scalable transfer of very fragile oxide thin film transistors. The TFT performance was investigated before and after mounting on the stretchable substrate. Further reliability of the TFTs was confirmed in stretching and cyclic tests. After transferring TFT arrays to the stretchable substrate, wrinkles in interconnecting bridges were formed, which gives stretchability to the circuitry without significant degradation of the TFT performance. The contact mechanics between the roller and the TFT arrays during the transferring process was explored, simulated, and correlated with the observed experimental results.

2. Device Fabrication Process and Roller Description

A schematic representation of IGZO TFT that indicates the various layers in the fabrication process is shown in **Figure 1**a. The annealing of germanium (Ge) on the SiO_2/Si substrate in an O_2 environment created GeO_2, which acts as a sacrificial layer. Indium tin oxide (ITO) was used as gate and source-drain (S-D) electrodes, while SiO_2 and IGZO were used as the gate dielectric and channel layer, respectively. IGZO TFTs were encapsulated by SU-8 epoxy rectangles, leaving a small opening for electrical contact and periodic openings among IGZO device islands exposing to SiO_2. An optical image of an SU-8-encapsulated IGZO TFT is shown in Figure 1b. After etching the SiO_2 and dissolving the GeO_2, the TFTs were ready for transfer. The transfer process of the TFTs consists of two steps: picking and placing. In the picking step, a thin polydimethylsiloxane (PDMS) film was attached to a stainless steel roller as a blanket (roll-stamp). The roller with the PDMS stamp was moved over the encapsulated IGZO TFT arrays on the Si substrate by optimizing the nip force between the substrate and the roller, as shown in Figure 1c. A magnified photo of the attached IGZO TFT arrays on the roller surface is shown in Figure 1d. Next, in the placing step, the roller with the TFT arrays attached was allowed to move on a receiving PDMS substrate for placing the TFT arrays. During the picking and placing steps, uniform nip pressure along roll axis and synchronization between the angular motion of the roller and the translational motion of the sample mounting stage are required.

The roller was made of steel and positioned on an axial rod, as shown schematically in **Figure 2**a. The complete

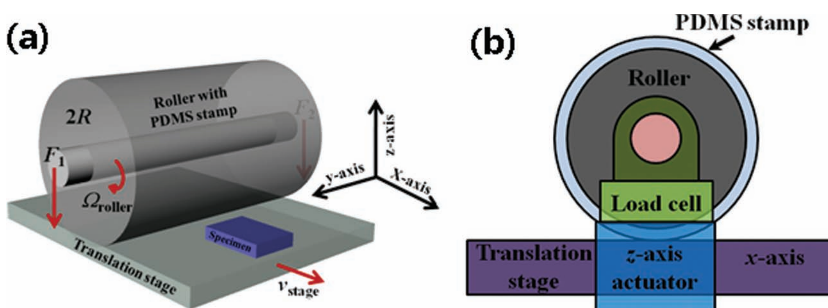

Figure 2. a) Schematic representation of roller transfer process. b) Schematic cross-sectional of the roller showing the position of load cell and actuator.

© 2013 WILEY-VCH Verlag GmbH & Co. KGaA, Weinheim

roller system can be controlled by a computer interface, and the magnitude and uniformity of the contact load can be precisely controlled by a feedback module with two load sensors and two z-axis actuators connected to the roller. The cross-sectional view of one end is shown in Figure 2b, to which load sensors and z-axis actuators are attached. The position parameter z (along the vertical axis) at two extreme ends decides the distribution of pressure along the roll axis, whereas x (along the translational motion) defines the motion of the roller along the forward direction. In the roll transfer process, two key factors must be considered: 1) uniform contact between the roller and the flat substrate, and 2) synchronization between the angular motion of the roller and translational motion of the sample mounting stage to avoid shear force that the device might experience during transfer. Uniform contact along the roll axis can be achieved by measurement of the nip force in real time with the help of load sensors at the two ends. In maintaining uniform nip pressure during the transfer process, the feedback system works by actuating two high-precision z-axis actuators at both ends of the roll axis. The automated roll system was calibrated to obtain uniform nip contact pressure. This load-controlled automated roller is capable of continuously transferring large-area electronic circuitry. The roller picks the devices from one plate and transfers them to a desired substrate on another plate. After that, it again moves to a previous plate for picking other electronic circuitry for transferring.

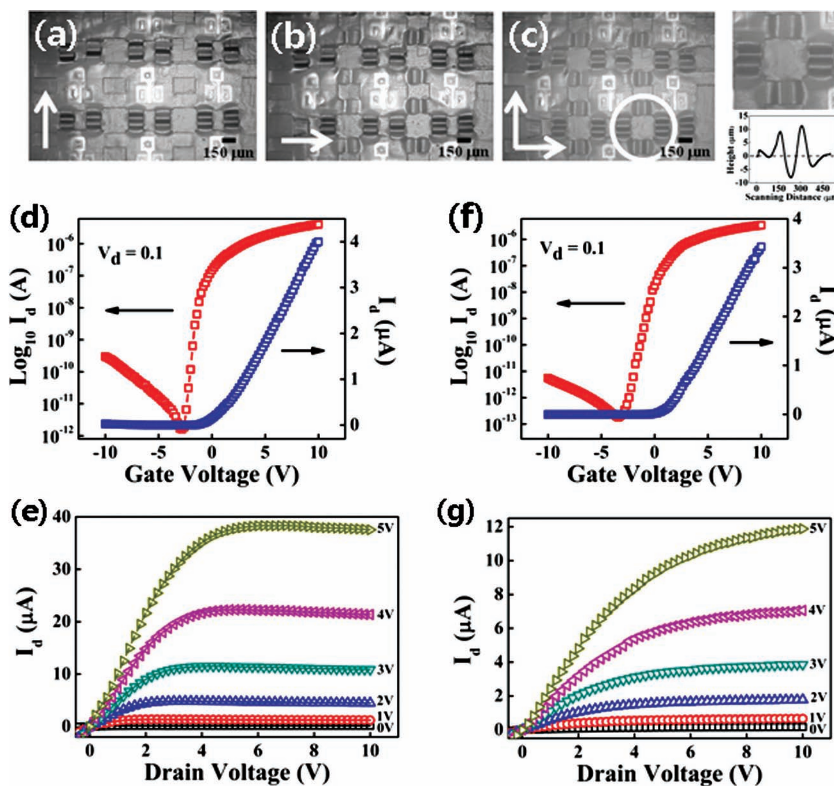

Figure 3. a–c) Observation of anisotropy in wrinkle formation, and electrical characteristics of IGZO TFT d,e) before and f,g) after the transfer onto the stretchable substrate. a) Wrinkle formation in the direction of roller motion (x-axis), indicated by the arrow. b) Wrinkle formation also starts along the y-axis. c) Wrinkles formed in both directions (x- and y-axes). Right side upper part shows zoomed image and lower part shows the amplitude. d) Transfer characteristics and e) output characteristics of IGZO TFT before the transfer (on the Si substrate). f) Transfer characteristics and g) output characteristics of IGZO TFT after transfer onto the stretchable substrate by the automated roller.

For transferring the IGZO TFTs, the diameter and width of the roller with the PDMS stamp was estimated as ≈150 mm. The optimized nip force for uniform contact pressure between the roll-stamp and the devices was found to be ≈10 N and the velocity of translation was kept at 1 mm/s during the picking step. The width of devices was considered to be ≈10 mm. While transferring the devices from the roller to the receiving stretchable substrate (placing step), the nip force and translation velocity were kept at 3 N and 0.1 mm/s, respectively.

3. Results and Discussion

3.1. Roller Motion on Stretchable Substrate: Wrinkle Formation

The receiving stretchable substrate was prepared by baking the PDMS solution in an oven (70 °C for 10–15 min), leaving it in a somewhat sticky state. After completing the placing process, wrinkles in the interconnecting bridges start to form on the receiving substrate, and this delayed development of wrinkles results from the viscoelastic behavior of the receiving substrate. Anisotropy was observed in the formation of wrinkles among the SU-8-encapsulated devices. This anisotropy can be explained as follows: initially, the PDMS receiving substrate was soft enough (at 70 °C) to deform, thus, during the placing process, it was stretched along the translational direction (x-axis) due to the nip pressure. As the roller with the TFTs attached moves on the receiving substrate attached to the translation stage, the stretched region of the receiving PDMS also moves in order to relax the previous region, and starts to form wrinkles in this direction. Therefore, immediately after completing the transfer process, wrinkles were observed in only this direction (the arrow indicates the direction of the roller motion and the formation of wrinkles) (**Figure 3**a). During the transferring process, the receiving substrate was maintained at almost ≈70 °C, and after completing the transfer process, it starts to cool uniformly (from 70 °C to room temperature), becoming hard and resulting in wrinkle formation along the y-axis (indicated by the arrow) (Figure 3b). Figure 3c shows an optical image of devices on a receiving stretchable PDMS substrate with the wrinkle formation in both directions (right side of Figure 3c, the upper part shows the zoomed image of a wrinkle, and the lower part shows its amplitude). The observed anisotropic effect can also

© 2013 WILEY-VCH Verlag GmbH & Co. KGaA, Weinheim

be further understood with the help of results obtained by finite element analysis, which will be discussed later.

3.2. Transfer and Output Characteristics

Linear and semi-logarithmic plots of transfer characteristics of IGZO TFT before and after the transfer at V_d = 0.1 V are shown in Figure 3d,f, respectively. Both the transfer curves revealed that IGZO TFTs can be very well operated in the low-voltage region (± 5 V) before and after the transfer process. The threshold voltage (V_{th}), field effect mobility (μ_{FE}), on-off ratio ($I_{on/off}$) and subthreshold swing (SS) before the transfer were estimated as ≈1.16 V, 15.00 $cm^2/V·s$, 0.2 × 10^7, and 0.28 V·decade^{-1}, respectively, whereas these parameters after the transfer by the roller were changed to ≈1.26 V, 12.83 $cm^2/V·s$, 1.8 × 10^7, and 0.33 V·decade^{-1}, respectively. This shows that after transferring the IGZO TFTs by the roller, V_{th} changed by 0.1 V, $I_{on/off}$ increased by one order of magnitude, the SS value changed from 0.28 to 0.33, and the mobility changed from 15.00 to 12.86 $cm^2/V·s$. The slight changes in IGZO TFT parameters are possibly due to the transfer process, which involves heating of the devices in water at 150 °C to dissolve the GeO_2 sacrificial layer. The OH-radicals of water can cause a slight decrease of the electrical conductivity of an oxide transistor.[34] In addition, the mechanical stress generated in the active layers of a device during attachment to the curved surface of the roller may also affect the device performance. However, the changes in IGZO TFT parameters may again be improved by more careful process optimization. The output characteristics of IGZO TFT before and after the transfer for various gate voltages (V_g = 0–5 V) are shown in Figure 3e,g, respectively. The linear behavior of the drain current in the low-V_d region of Figure 3e indicates that the source/drain-channel interface contact is ohmic, which is maintained even after employing the transferring process (Figure 3g).

To further explore the feasibility of the automated roll transfer process in flexible and stretchable electronics, devices are tested in stretching and cyclic tests with the help of a stretching machine. The two ends of the IGZO TFTs mounted on PDMS substrate were fixed in the stretching machine in such a way that stretching can be performed along the channel length. As the elastic substrate was stretched, the interconnected bridges among IGZO devices consume almost all external strain by reducing their amplitude, as these parts are softer than the encapsulated rectangles of active devices. **Figure 4**a shows the transfer curves of an IGZO TFT in linear and semi-logarithmic scale with increasing stretching values from 0 to 5%, at 1% intervals and 0.1-V drain voltage (V_d). The IGZO TFT showed good stability under the maximum stretching level of 5%, as no significant changes were observed in TFT parameters. The variation of V_{th} and μ_{FE} is shown in Figure 4b, indicating that V_{th} (1.26–1.7) and μ_{FE} (12.83–11.79) change slightly. The output characteristics of the IGZO TFT at a maximum stretching level of ≈5% for different gate voltages (V_g = 0–5 V) are shown in Figure 4c. The linear behavior of the drain current (I_d) in the low-V_d region showed mechanical robustness of the source/drain electrode contacts with the IGZO channel layer under stretching test. The mechanical endurance capability of the IGZO TFTs was also explored by measuring the TFT characteristics under repeated cyclic tests. Figure 4d shows the transfer curves of an IGZO TFT in linear and semi-logarithmic scale for 20, 40, 60, 80, and 100 repeated cycles at V_d = 0.1 V. The variation of V_{th} and μ_{FE} under repeated cycles is shown in Figure 4e. Under repeated cyclic tests, V_{th} (1.04–1.25) and μ_{FE} (12.2–10.12) change slightly. The output characteristics of the IGZO TFT at 100 repeated cycles for different gate voltages (V_g = 0–5 V) are shown in Figure 4f, which again indicate the consistent performance of the device, without any degradation. The low SS value indicates that the IGZO TFTs can be very well operated within the small gate voltage region (±5 V), even under stretching and cyclic tests, which can be clearly observed in the transfer curves shown in Figure 4a,d. The variation of $I_{on/off}$ and SS for 0–5% stretching and various repeated cycles is shown in **Figure 5**a,b, respectively. All the TFT parameters are summarized in **Table 1**, for before (on the Si substrate) and after the transfer (on the stretchable substrate), and under stretching and cyclic tests. Careful observation shows that during the complete measurement, the maximum possible change in V_{th} is ≈1.23 ± 0.5 V, that in $I_{on/off}$ is ≈(2.3 ± 2.1) x 10^7, and the SS value changes within the range of 0.5 ± 0.2 V·decade^{-1}. The mobility decreases slightly under stretching, while it is maintained at up to 10 $cm^2/V·s$ for 100 repeated cycles. It was revealed that the IGZO TFT shows good stability and durability on the PDMS stretchable substrate after transferring by the automated roller. It is also notable that in the measurement of the TFT on the soft stretchable substrate, hard contact tips sometimes tear the electrodes, resulting in the same device showing slightly poorer electrical performance. This could also be one of the reasons for the observation of the slight fluctuation of the electrical parameters in the present study.

3.3. Mechanics Involved in Roll-Transfer Process: Numerical Simulation

To understand the various key factors involved in the roll transfer process and how these can affect the device properties, numerical simulations were carried out using bending theory and finite element analysis. For the simulation, there are three possibilities for considering the active layers in the IGZO TFT device (**Figure 6**a). We considered all the active layers (case 2, Figure 6a), including ITO (gate), SiO_2 (dielectric), IGZO (channel) and ITO (S-D). To obtain the applied strain value for each layer, the location of the neutral axis of the device layers is calculated using bending theory. Accordingly, the normal longitudinal strain is given by $\varepsilon = -y/\rho$, where y is the distance from the neutral axis and ρ is the radius of the bending curvature. The position of the neutral axis for composite film is calculated using the following equation:

$$y_c = \frac{\sum_i y_i E_i t_i}{\sum_i E_i t_i} \quad (1)$$

Here, E_i is the Young's modulus of the i-th layer in the composite film, and t_i represents its thickness. y_i is the centroidal point of each film, which can be expressed by $y_i = \left(\sum_{j=1}^{i} t_j\right) - t_i/2$. The position of the neutral axis, y_c, can be

© 2013 WILEY-VCH Verlag GmbH & Co. KGaA, Weinheim

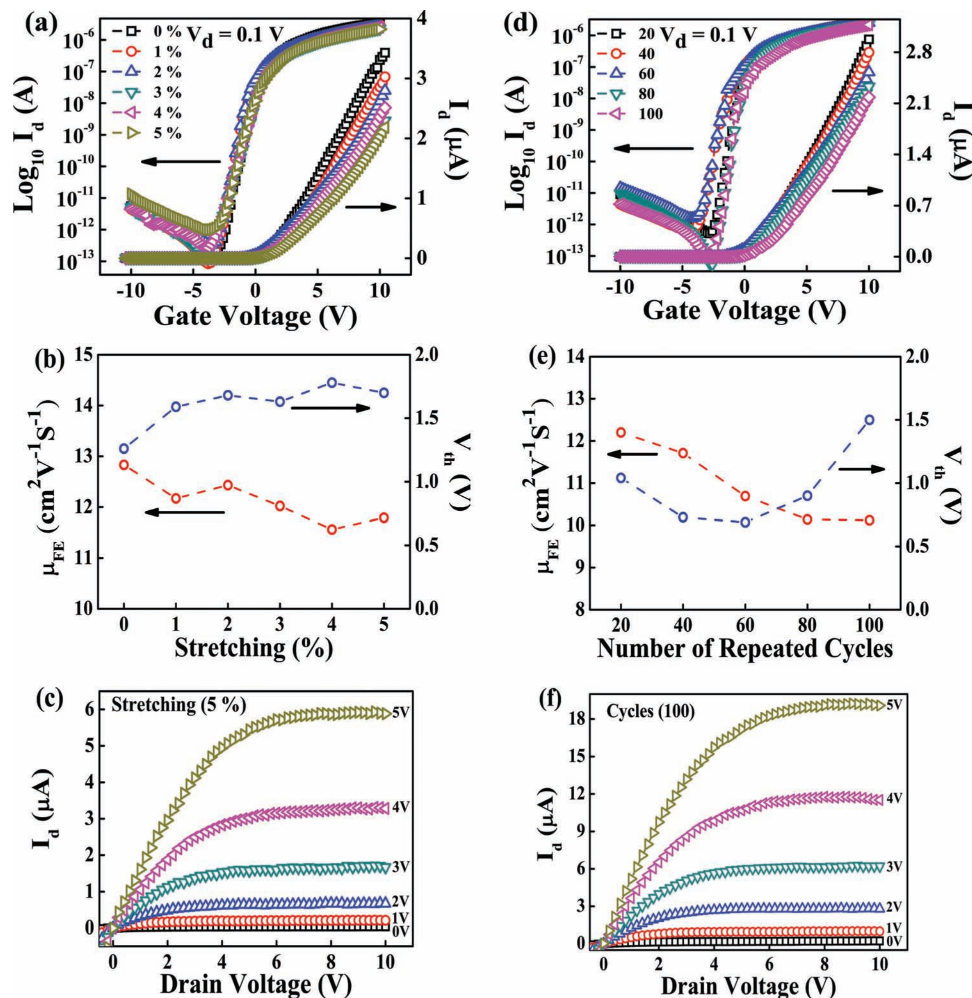

Figure 4. Electrical performance of IGZO TFT on stretchable substrate under a–c) stretching and d–f) repeated cyclic tests. a) Transfer characteristics at different stretching levels (0–5%). b) Variation of mobility (μ_{FE}) and threshold voltage (V_{th}) under different stretching values (0–5%). c) Output characteristics at different gate voltages (V_g = 0–5 V) for a maximum stretching value of 5%. d) Transfer characteristics in various repeated cyclic tests (20, 40, 60, 80, and 100). e) Variation of mobility (μ_{FE}) and threshold voltage (V_{th}) under repeated cyclic tests. f) Output characteristics at different gate voltages (V_g = 0–5 V) for 100 repeated cycles.

characterized from the bottom surface, and then the bending strain of the *i*-th film can be calculated from:

$$\varepsilon_i = \frac{y_i - y_c}{\rho} \tag{2}$$

There are two representative kinds of interface between the roll-stamp and the device top layer. If we assume that the devices can freely slide on the surface of the roll-stamp, i.e., the sliding interface (upper part, Figure 6b), the friction between the devices and the roller can be ignored. In this case, the neutral axis can be obtained by considering the bending problem of the composite film without any supported materials. Hence, the position of the neutral axis is calculated as y_c = 548.0 nm (Figure 6c) using Equation (1). On the other hand, if we consider that the devices are perfectly bonded on the surface of the roller, i.e., the perfectly bonded interface (lower part, Figure 6b), the device will bend and be

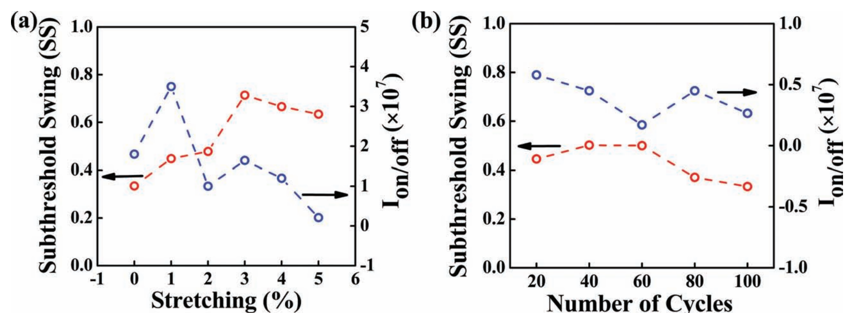

Figure 5. a) Variation of subthreshold swing (SS) and on-off ratio ($I_{on/off}$) with respect to different stretching values (0–5%). b) Variation of subthreshold swing (SS) and on-off ratio ($I_{on/off}$) with respect to repeated cyclic tests.

© 2013 WILEY-VCH Verlag GmbH & Co. KGaA, Weinheim

Table 1. Electrical parameters: threshold voltage (V_{th}), on-current (I_{on}), off-current (I_{off}), on-off ratio ($I_{on/off}$), subthreshold swing (SS) and mobility (μ_{FE}) of IGZO TFT before transfer (on Si substrate) and after transfer (on stretchable substrate, under stretching (0, 1, 2, 3, 4, and 5%) and under repeated cyclic tests (20, 40, 60, 80, and 100)).

Parameters	Before	After	Stretching [%]					Number of Repeated Cycles				
			1	2	3	4	5	20	40	60	80	100
V_{th} (V)	1.16	1.26	1.59	1.68	1.63	1.78	1.7	1.04	0.73	0.69	0.9	1.25
I_{on} (A)	4.1×10^{-6}	3.3×10^{-6}	2.9×10^{-6}	2.9×10^{-6}	2.2×10^{-6}	2.3×10^{-6}	2.1×10^{-6}	2.8×10^{-6}	2.8×10^{-6}	2.5×10^{-6}	2.2×10^{-6}	2.1×10^{-6}
I_{off} (A)	1.6×10^{-12}	1.8×10^{-13}	1.0×10^{-13}	3.3×10^{-13}	1.3×10^{-13}	2.4×10^{-13}	1.0×10^{-12}	4.9×10^{-13}	6.2×10^{-13}	1.4×10^{-12}	5.0×10^{-14}	8.1×10^{-14}
$I_{on/off}$	0.2×10^{7}	1.8×10^{7}	2.9×10^{7}	0.8×10^{7}	1.6×10^{7}	0.9×10^{7}	0.2×10^{7}	0.5×10^{7}	0.4×10^{7}	0.2×10^{7}	4.4×10^{7}	2.5×10^{7}
SS (V/decade)	0.28	0.33	0.44	0.47	0.71	0.66	0.63	0.44	0.50	0.5	0.37	0.33
μ_{FE} (cm^2/Vs)	15.00	12.83	12.17	12.43	12.02	11.56	11.79	12.2	11.71	10.69	10.14	10.12

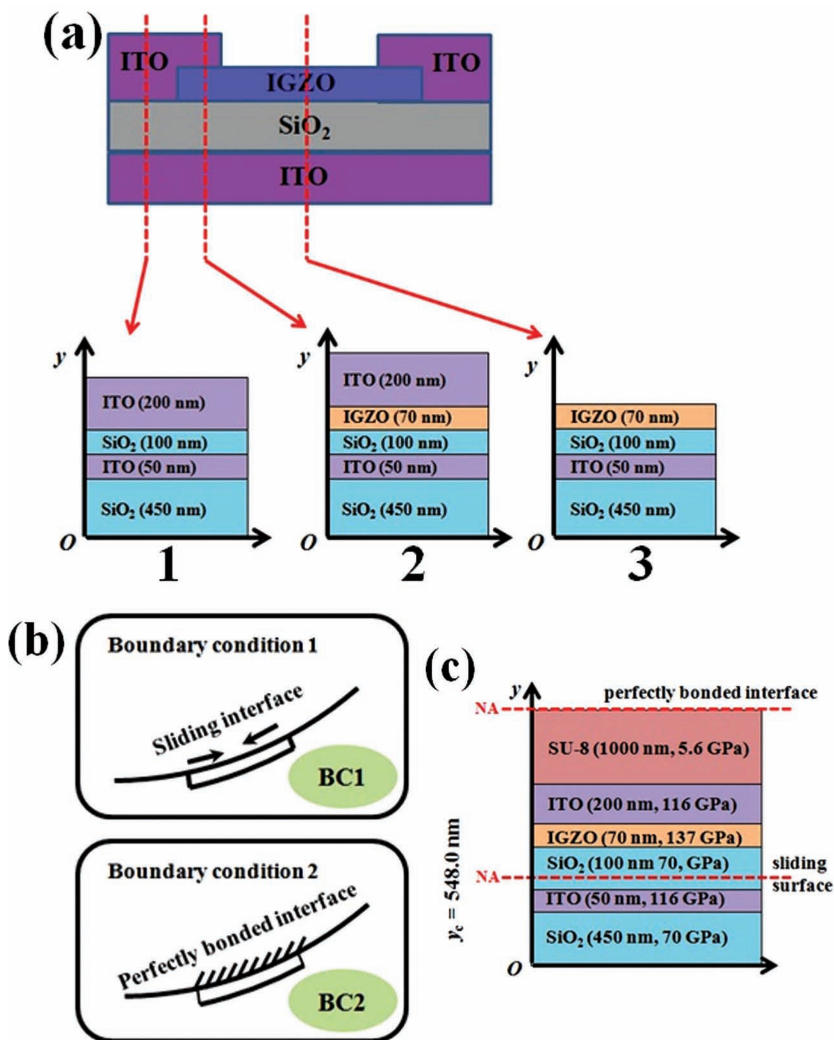

Figure 6. a) Cross-sectional schematic of IGZO TFT showing active layers at different regions. b) Sliding interface and perfectly bonded interface. c) Position of neutral axis for the sliding case is located at SiO_2 (gate dielectric) and for the perfectly bonded case is positioned at the top surface of the device.

attached on the surface. When the roller is rolling on the flat surface of the device, the surface of the devices will successively contact the roller. Therefore, we can regard the strain of the top surface of the devices as zero in the perfectly bonded case. From the definition of the neutral axis, the position of the neutral axis is equal to the position of the top SU-8 surfaces, i.e., y_c = 1870 nm (Figure 6c). After deciding the position of the neutral axis, the strain values are calculated for all device active layers for both the cases using Equation 2 (shown in **Figure 7**c).

When the roller is allowed to move on the device on a Si substrate (Figure 7a), the PDMS stamp attached to the roller surface deforms due to the contact pressure. This deformation leads to a complicated distribution of tension and compression strains at and near the contacted area of the roller and substrate. To understand the exact nature of deformation, the tangential strain and contact pressure were calculated with the circumferential distance, as shown in Figure 7b. The values of Young's modulus and Poisson's ratio of the PDMS roll-stamp used for the calculation were 2 MPa and 0.5, respectively. The variation in the strain value for the PDMS stamp can be divided into two regions: one from the center to the contact boundary, and the other beyond the contact boundary. At the center of the contact area, the PDMS stamp experiences a maximum tensile strain of ≈0.7%. As we go from the contact center to the contact boundary along the circumferential distance, the tensile strain decreases to zero, and after that, the compressive strain increases to an extent, and decreases to zero at the contact boundary. Beyond the contact boundary, the compressive strain first increases and then

© 2013 WILEY-VCH Verlag GmbH & Co. KGaA, Weinheim

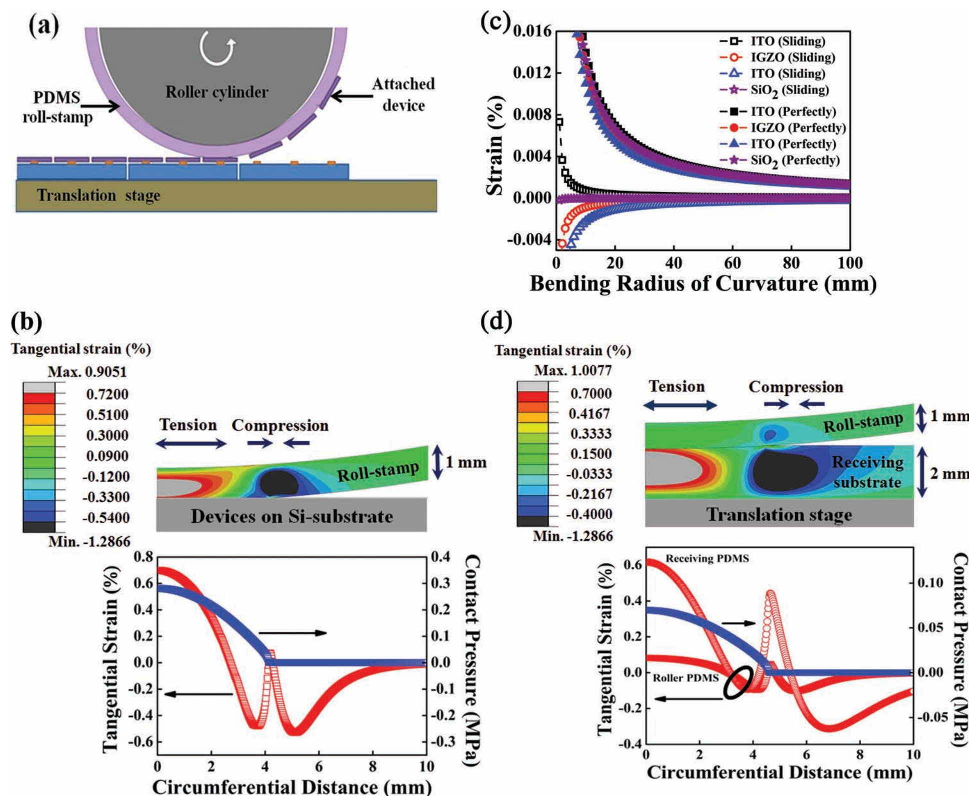

Figure 7. a) Schematic of roller motion on the stretchable, receiving substrate. b) Variation of simulated strain and contact pressure values due to the deformation of the roll-stamp with respect to the circumferential distance from center of contact area during the picking of devices by the automated roller. c) Calculated strain values with respect to the bending radius of curvature for a perfectly bonded and a sliding surface. d) Variation of simulated strain and contact pressure values due to the deformation of the roll-stamp and receiving substrate with respect to the circumferential distance from the center of the contact area during the placing of devices from the automated roller.

decreases to zero, after which there is no strain along the circumference far away from the contact boundary. When the device is attached to the PDMS stamp during the picking step, the active layers of the device experience in-plane strain due to the radius of curvature of the roller. Concerning the interface configuration between the PDMS stamp and a device, there are two major possibilities: either the PDMS stamp can be perfectly bonded with the device's top encapsulated layer, or it can slide on the top surface of the device. The calculated strain values in the device active layers for these two conditions with respect to the radius of curvature are shown in Figure 7c. For the sliding case, the S-D electrodes (ITO) and channel (IGZO) experienced compressive strain, whereas that of the gate electrode (ITO) was tensile strain. This is because the neutral axis for the sliding case lies on SiO_2 (a dielectric), which experiences almost no strain. In this case, the calculated strain values of the device active layers for a 75-mm radius are almost negligible, which indicates that the device is not affected, if this is the case. In the case of perfect attachment, the neutral axis was found to be at the top encapsulated layer of the device, so all active layers experienced tensile strain. In this case, the strain level sharply increases below the bending radius of ≈20 mm, whereas above this radius, its value decreases and becomes almost saturated for a large radius of curvature (≥60 mm). In the present study, a roller with a radius of ≈75 mm was employed, which could provide a maximum strain of ≈0.2% for a perfectly bonded case in device active layers (Figure 7c), well below the maximum fracture strain of the active layers and providing almost no strain for the sliding case. It is inferred that the active layers of the device maintain mechanical robustness after the attachment to the roller surface, regardless of bonded conditions. During the transfer of devices from the roller to the receiving substrate, the PDMS, the roll-stamp and the receiving substrate can deform. The receiving substrate deforms more than the roll-stamp, as it is sufficiently softened and sticky. Similar calculations of the tangential strain (resulting from deformation) and contact pressure between the roller and the receiving PDMS with circumferential distance were carried out to estimate the strain distribution in both PDMS. The Young's modulus of the receiving substrate used for calculation was 0.8 MPa, which is much smaller than the roll-stamp (2 MPa). The strain level in the receiving PDMS was found to be much higher than that in the roll-stamp, as shown in Figure 7d. The maximum tensile strain was found to be at the center of the contact area, and as the roller moves, this strain is also propagated in the forward direction, leaving the previous position in a relaxed state. The relaxing of the receiving PDMS substrate in the direction of roller motion starts to create wrinkles in this direction (Figure 3a). After completing the rolling, it starts to shrink in a 2D plane, and wrinkles form in all directions (Figures 3b,c).

© 2013 WILEY-VCH Verlag GmbH & Co. KGaA, Weinheim

This discussion shows that during the picking and placing steps, the induced strain is not sufficient to affect the mechanical robustness and electrical performance of the devices. On the other hand, the strain generated due to the deformation of the receiving PDMS substrate in the transfer of the devices from the roller to the receiving substrate is effectively utilized in creating the wrinkle patterns, providing stretching ability. Therefore, the roll transfer process seems to be more practical and realistic for transferring and scaling up inorganic-based devices from high-temperature-resistant Si substrates to flexible/stretchable substrates.

4. Conclusions

In summary, stretchable and transparent IGZO TFTs with high electrical performance were demonstrated based on a scalable manufacturing method of load-controlled roll transfer. To secure high electrical performance, these devices were fabricated on a conventional Si substrate, then integrated on a stretchable substrate using the roll transfer system. After integration, IGZO TFTs showed high electrical performance under stretching and cyclic tests. To assure the scalability of the roll transfer method, the contact load between the roller and the devices should be precisely controlled during the transfer process, and a unique mechanism for controlling the contact load was developed by incorporating the load sensors and actuators in the roller. The mechanics involved in the roll transfer process was investigated and simulated, which showed that the strain level experienced by the active layers of the device was controlled to well below their maximum fracture level. The feasibility of the load-controlled roll system was explored for transferring the inorganic devices from rigid to flexible or stretchable substrates without affecting the electrical performance, presenting a new method for large-area production in the field of flexible and stretchable electronics.

5. Experimental Section

Device Fabrication: Si substrate was cleaned successively with acetone, isopropyl alcohol, and deionized water using an ultrasonic bath. 300-nm germanium (Ge) and 450-nm silicon dioxide (SiO_2) layers were deposited with an e-beam evaporator. The substrate deposited with Ge and SiO_2 was annealed in an O_2 environment at 450 °C for 2 h, creating a GeO_2 layer between Ge and SiO_2, acting as a sacrificial layer. A ≈50-nm indium tin oxide layer (ITO) was deposited as a gate electrode with Ar = 30 sccm by sputter coating, and ≈100 nm of SiO_2 was deposited as a gate dielectric by plasma-enhanced chemical vapor deposition (PECVD). Afterwards, an ≈80-nm IGZO channel layer (4-inch circular target: In:Ga:Zn = 1:1:1) was deposited with Ar/O_2 = 38/2 sccm by sputtering method, and gate openings were produced by SiO_2 etching. The ITO (≈150 nm) was deposited by sputter coating as source-drain electrodes and for the gate contact. The channel length (L) and width (W) for TFTs were defined as 20 μm and 200 μm, respectively. For patterning the gate electrode ITO, channel layer IGZO, and source-drain electrode ITO, a conventional photolithographic method with photoresist material AZ 5214 was used, and each layer was deposited by RF-sputtering with a power density of ≈100 Wcm^{-2} and pressure of ≈150 mTorr, followed by lift-off. After depositing each layer, heat treatment was performed at 350 °C for 1 h in order to stabilize and improve the electrical conductivity.

Roll Transferring Process: For transferring the IGZO-based TFT arrays using the roller, the following steps were followed. First, the encapsulating layer SU-8 (50%) was spin coated and patterned in such a way that devices were covered by SU-8 rectangles, with small openings at the Gate and S-D regions for electrical contact, and these rectangles were interconnected by bridges with periodic regular openings exposing the SiO_2. The exposed SiO_2 was etched by reactive ion etching method, using CHF_3 and O_2 gases with a ratio of 7:1 and power density of ≈100 W cm^{-2}, until the GeO_2 sacrificial layer was exposed. During the etching of SiO_2 by plasma, the encapsulating layer of SU-8 can be damaged, so to protect it, the photoresist material was spin coated and subjected to the same pattering. After etching the SiO_2, the PR was removed by acetone, and the TFT arrays were rinsed with deionized water. PDMS thin film was attached to the surface of the roller, and TFT arrays encapsulated by the SU-8 layer were heated in deionized water for 1 h at 150 °C to dissolve the GeO_2 sacrificial layer. For attaching the TFT arrays to the roller surface (picking step), TFT arrays were placed on a translation stage, and the roller was allowed to move over them slowly by optimizing the nip force between the substrate and the roller, with synchronization between the angular motion of the roller and the translational motion of the sample mounting stage. The receiving substrate was prepared by making the PDMS solution and baking it in a vacuum oven at 70 °C for 10–15 min, leaving it in a somewhat sticky state. After that, the roller with the TFT arrays attached was allowed to move on the receiving PDMS substrate for transferring the TFT arrays. After transferring the TFT arrays, wrinkle formation was observed in the interconnecting bridges among the TFT islands.

Electrical Measurements: The TFT characteristics were measured before and after transferring the devices. Stretching and cyclic measurements were carried out using a stretching machine. For measuring the TFT characteristics, a probe station coupled with a semiconductor characterization system was used (Keithley: 4200-SCS).

Finite Element Method (FEM): The simulation of contact problems between the roller and flat substrate was performed by finite element analysis using ABAQUS. In the picking step, a deformable roll-stamp picks the devices from a rigid substrate, and the devices experience in-plane strain due to bending deformation. 2-dimensional finite element models were simulated to obtain the in-plane strain with a roll-stamp of 1-mm thickness and Young's modulus of 2 MPa during the picking step. In addition, it was assumed that the stamp and substrate contact was frictionless. Under this assumption, we can obtain the maximum local strain value that the devices will experience during the picking step. In the placing step, the devices attached to the roll-stamp were transferred to 2-mm-thick PDMS substrate. The Young's modulus of the receiving PDMS substrate used was 0.8 MPa for the simulation, which is smaller than the roll-stamp, because the receiving substrate was not fully cured in order to enhance the adhesion between the devices and the substrate. The frictionless contact condition was also assumed at the interface between the stamp and the receiving substrate as in the picking step. The contact forces per unit roller length for the picking and placing steps are 1 and 0.3 N/mm, respectively. These two models have the symmetric plane that is defined by the centerline of the contact area and the axis of the roll-stamp. In the two-dimensional FEM models, the left side shown in the strain variation of Figure 7b,d is the symmetric plane. From the contact simulation, the strain distribution of the circumferential direction was obtained, which shows the deformation of the stamp and the substrate causing wrinkling phenomena during the transfer process.

Acknowledgements

This work was supported by Research Program (No. 2012R1A2A1A03006049, 2009-0064888, 2009-0083540) and Global Frontier Research Center for Advanced Soft Electronics (No. 2011-0031635) through the National Research Foundation of Korea (NRF), funded by the Ministry of Education, Science and Technology, and a Grant-in-Aid for Industrial Source Technology Development Programs from the Korea Ministry of Knowledge Economy (No. 10033309).

Received: September 3, 2012
Published online: November 14, 2012

© 2013 WILEY-VCH Verlag GmbH & Co. KGaA, Weinheim

[1] T. Kamiya, H. Hosono, *NPG Asia Mater.* **2010**, *2*, 15.
[2] J.-S. Park, T.-W. Kim, D. Stryakhilev, J.-S. Lee, S.-G. An, Y.-S. Pyo, D.-B. Lee, Y. G. Mo, D.-U. Jin, H. K. Chung, *Appl. Phys. Lett.* **2009**, *95*, 013503.
[3] M. Ito, M. Kon, C. Miyazaki, N. Ikeda, M. Ishizaki, Y. Ugazin, N. Sekine, *IEICE Trans. Electron.* **2007**, *E90-C*, 2105.
[4] Z. Yu, X. Niu, Z. Liu, Q. Pei, *Adv. Mater.* **2011**, *23*, 3989.
[5] R. Carta, P. Jourand, B. Hermans, J. Thone, D. Brosteaux, T. Vervust, F. Bossuyt, F. Axisa, J. Vanfleteren, R. Puers, *Sens. Actuators, A* **2009**, *156*, 79.
[6] F. Axisa, D. Brosteaux, E. D. Leersnyder, F. Bossuyt, J. Vanfleteren, B. Hermans, R. Puers, Proc. 29th Annual International Conference of the IEEE EMBS, Lyon, France **2007**, 5687.
[7] F. Axisa, F. Bossuyt, T. Vervust, J. Vanfleteren, 2nd Electronics Systemintegration Technology Conference, Greenwich, UK **2008**, 1387.
[8] S. G. Lee, D. Y. Lee, H. S. Lim, D. H. Lee, S. Lee, K. Cho, *Adv. Mater.* **2010**, *22*, 5013.
[9] G. A. Niklasson, C. G. Granqvist, *J. Mater. Chem.* **2007**, *17*, 127.
[10] K. Cherenack, C. Zysset, T. Kinkeldi, N. Munzenrieder, G. Troster, *Adv. Mater.* **2010**, *22*, 5178.
[11] J. Coosemans, B. Hermans, R. Puers, *Sens. Actuators, A* **2006**, *130-131*, 48.
[12] C. Zysset, N. Munzenrieder, T. Kinkeldi, K. Cherenack, G. Troster, *IEEE Electron Device Lett.* **2012**, *59*, 721.
[13] E. R. Post, M. Orth, P. R. Russo, N. Gershenfeld, *IBM Syst. J.* **2000**, *29*, 840.
[14] T. Kinkeldi, C. Zysset, K. Cherenack, G. Troester, *IEEE Sensors Conf.* **2009**, 1580.
[15] S.-H. K. Park, C. S. Hwang, M. Ryu, S. Yang, C. Byun, J. Shin, J.-I. Lee, K. Lee, M. S. Oh, S. Im, *Adv. Mater.* **2009**, *21*, 678.
[16] J. S. Park, W.-J. Maeng, H.-S. Kim, J.-S. Park, *Thin Solid Films* **2012**, *520*, 1679.
[17] J. Liu, D. B. Buchholz, J. W. Hennek, R. P. H. Chang, A. Facchetti, T. J. Marks, *J. Am. Chem. Soc.* **2010**, *132*, 11934.
[18] K. Nomura, T. Kamiya, H. Hosono, *Adv. Mater.* **2011**, *23*, 3431.
[19] H. Q. Chiang, J. F. Wager, R. L. Hoffman, J. Jeong, D. A. Keszler, *Appl. Phys. Lett.* **2005**, *86*, 013503.
[20] E. Fortunato, P. Barquinha, R. Martins, *Adv. Mater.* **2012**, *24*, 2945.
[21] P. Wellenius, A. Suresh, H. Luo, L. M. Lunardi, J. F. Muth, *J. Disp. Technol.* **2009**, *5*, 438.
[22] K. Nomura, H. Ohta, A. Takagi, T. Kamiya, M. Hirano, H. Hosono, *Nature* **2004**, *432*, 488.
[23] T. Kamiya, K. Nomura, H. Hosono, *Sci. Technol. Adv. Mater.* **2010**, *11*, 044305.
[24] K. H. Cherenack, N. Munzenrieder, G. Troster, *IEEE Electron Device Lett.* **2010**, *31*, 1254.
[25] S. Jeong, Y.-G. Ha, J. Moon, A. Facchetti, T. J. Marks, *Adv. Mater.* **2010**, *22*, 1346.
[26] N. Munzenrieder, K. H. Cherenack, G. Troster, *IEEE Trans. Electron Devices* **2011**, *58*, 2041.
[27] D.-H. Kim, J. Song, W. M. Choi, H.-S. Kim, R.-H. Kim, Z. Liu, Y. Y. Huang, K.-C. Hwang, Y.-W. Zhang, J. A. Rogers, *Proc. Natl. Acad. Sci. USA* **2008**, *105*, 18675.
[28] D.-H. Kim, N. Lu, R. Ma, Y.-S. Kim, R.-H. Kim, S. Wang, J. Wu, S. M. Won, H. Tao, A. Islam, K. J. Yu, T.-I. Kim, R. Chowdhury, M. Ying, L. Xu, M. Li, H.-J. Chung, H. Keum, M. McCormick, P. Liu, Y.-W. Zhang, F. G. Omenetto, Y. Huang, T. Coleman, J. A. Rogers, *Science* **2011**, *333*, 838.
[29] S. Bae, H. Kim, Y. Lee, X. Xu, J.-S. Park, Y. Zheng, J. Balakrishnan, T. Lei, H. R. Kim, Y. Song, Y.-J. Kim, K. S. Kim, B. Ozyilmaz, J.-H. Ahn, B. H. Hong, S. Iijima, *Nat. Nanotechnol.* **2010**, *5*, 574.
[30] M. H. Lee, N. Lim, D. J. Ruebusch, A. Jamshidi, R. Kapadia, R. Lee, T. J. Seok, K. Takei, K. Y. Cho, Z. Fan, H. Jang, M. Wu, G. Cho, A. Javey, *Nano Lett.* **2011**, *11*, 3425.
[31] L. Tavares, J. Kjelstrup-Hansen, H. Rubahn, *Small* **2011**, *7*, 2460.
[32] Y. Yang, Y. Hwang, H. A. Cho, J.-H. Song, S.-J. Park, J. A. Rogers, H. C. Ko, *Small* **2011**, *7*, 484.
[33] K. Park, D.-K. Lee, B.-S. Kim, H. Jeon, N.-E. Lee, D. Whang, H.-J. Lee, Y. J. Kim, J. H. Ahn, *Adv. Funct. Mater.* **2010**, *20*, 3577.
[34] G. Sengupta, H. S. Ahluwalia, S. P. Sen, *J. Colloid Interface Sci.* **1979**, *69*, 217.

© 2013 WILEY-VCH Verlag GmbH & Co. KGaA, Weinheim